Spin-Echo fMRI in Humans Using High Spatial Resolutions and High Magnetic Fields

Essa Yacoub,* Timothy Q. Duong, Pierre-Francois Van De Moortele, Martin Lindquist, Gregor Adriany, Seong-Gi Kim, Kâmil Uğurbil, and Xiaoping Hu

The Hahn spin-echo (HSE)-based BOLD effect at high magnetic fields is expected to provide functional images that originate exclusively from the microvasculature. The blood contribution that dominates HSE BOLD contrast at low magnetic fields (e.g., 1.5 T), and degrades specificity, is highly attenuated at high fields because the apparent T_2 of venous blood in an HSE experiment decreases quadratically with increasing magnetic field. In contrast, the HSE BOLD contrast is believed to arise from the microvasculature and increase supralinearly with the magnetic field strength. In this work we report the results of detailed and quantitative evaluations of HSE BOLD signal changes for functional imaging in the human visual cortex at 4 and 7 T. This study used high spatial resolution, afforded by the increased signal-to-noise ratio (SNR) of higher field strengths and surface coils, to avoid partial volume effects (PVEs), and demonstrated increased contrast-to-noise ratio (CNR) and spatial specificity at the higher field strengths. The HSE BOLD signal changes induced by visual stimulation were predominantly linearly dependent on the echo time (TE). They increased in magnitude almost quadratically in going from 4 to 7 T when the blood contribution was suppressed using Stejskal-Tanner gradients that suppress signals from the blood due to its inhomogeneous flow and higher diffusion constant relative to tissue. The HSE signal changes at 7 T were modeled accurately using a vascular volume of 1.5%, in agreement with the capillary volume of gray matter. Furthermore, high-resolution acquisitions indicate that CNR increased with voxel sizes < 1 mm³ due to diminishing white matter or cerebrospinal fluid-space vs. gray matter PVEs. It was concluded that the high-field HSE functional MRI (fMRI) signals originated largely from the capillaries, and that the magnitude of the signal changes associated with brain function reached sufficiently high levels at 7 T to make it a useful approach for mapping on the millimeter to submillimeter spatial scale. Magn Reson Med 49:655–664, 2003. © 2003 Wiley-Liss, Inc.

Key words: BOLD; fMRI; high fields; spin echo; brain; functional mapping; cerebral function

Functional parcellation in the brain is known to exist at a much finer spatial scale than the several-millimeter voxel dimensions currently used in functional imaging studies. However, initiatives aimed at functional mapping on such a scale are confronted with questions about the specificity (i.e., the accuracy of the maps relative to the actual boundaries of altered neuronal activity) and the magnitude of the imaging signals. Currently, most functional MRI (fMRI) studies in humans employ T_2^*-weighted, gradient-echo (GRE) BOLD fMRI because it provides the highest contrast-to-noise ratio (CNR) and is the easiest to implement. T_2^*-weighted BOLD signals at low fields were shown to be dominated by contributions from large draining veins (1–6) that can be distant from the activated site, with no evidence of a capillary contribution (3). Even at 4 T (7) and 4.7 T (8), large vein contributions are prominent. At higher magnetic fields, such as 7 T, the contribution of large vessels to GRE BOLD decreases *relative* to the microvasculature, due to the relatively higher capillary contribution and the suppression of intravascular BOLD signals caused by the dramatically shorter apparent T_2 of blood (Refs. 9 and 10, and references therein). However, blood vessels larger than capillaries on the venous side continue to contribute to T_2^*-weighted images even at 7 T (11) because of the extravascular BOLD effect that persists at all field strengths and increases linearly with the field magnitude. In addition, the shorter echo times (TEs) that must be used in T_2^*-weighted images lead to suboptimal capillary contribution and incomplete suppression of intravascular effects, while they maximize the BOLD effect from the larger venules and veins.

Initial increases in deoxyhemoglobin content (detected by T_2^* BOLD fMRI as a negative signal change) have spatial specificity on the millimeter to submillimeter scale (8,12–14). However, the fMRI signal changes associated with this transient phenomenon are small and difficult to detect, which limits its use as a general MRI approach. Perfusion changes also have been shown to have sufficient specificity to generate maps of iso-orientation columns in the cat visual cortex (15). Although it is better than the transient early negative BOLD effect, the CNR of perfusion-based functional maps is still relatively poor, and multislice coverage with this approach is limited.

An alternative approach for obtaining high-specificity functional images is Hahn spin-echo (HSE)-weighted BOLD at very high magnetic fields. HSE BOLD contrast arises because of diffusion-induced *dynamic* averaging of field inhomogeneities generated by deoxyhemoglobin-containing compartments (4,16,17). As such, HSE BOLD contrast has (in principle) both intra- and extravascular components, and only the latter is restricted to the microvasculature. The intravascular mechanism operative in HSE

BOLD is the averaging of the magnetic field inhomogeneities experienced by blood water as it diffuses around and exchanges across red cell membranes. This blood contribution is the dominant contribution at 1.5 T (1,18,19), and can account for as much as half the HSE functional image signal changes at 3 T (20). However, at very high fields, the apparent[1] T_2 of venous blood in an HSE experiment (9,21) becomes so short that the MR signal from the blood itself becomes diminishingly small. Therefore, with HSE BOLD fMRI at very high fields, only microvascular contributions originating predominantly from the extravascular BOLD effect are expected. This was found to be the case at 9.4 T in the rat somatosensory cortex (22).

Thus, ultra-high-field HSE BOLD can in principle improve the specificity of functional maps over GRE BOLD at the same field strength by eliminating the residual, extravascular BOLD effect originating from the veins, and by more complete suppression of the less-specific intravascular effects resulting from the use of longer TEs. Compared to lower field strengths, ultra-high fields can provide much needed improvements in the magnitude of the capillary signals in order for this approach to become a robust imaging method for high-resolution functional mapping. Microvascular HSE BOLD effects associated with changes in neuronal activity are intrinsically small, and are thought to be absent at 1.5 T (3). It is believed that they increase supralinearly with magnetic field magnitude[2] (4,16,17), but this has not been experimentally evaluated to date. If that hypothesis is correct, simultaneous improvements in CNR and specificity with increasing magnetic fields may enable HSE BOLD to become the preferred functional imaging approach at high (but not low) magnetic fields in experiments regarding high-resolution functional organization.

In this study, we examine the magnetic field and TE dependence of HSE BOLD signals for functional imaging with and without suppression of blood signals, using Stejskal-Tanner (S-T) gradients[3] (23) for the first time at a field strength significantly higher (7 T) than those used in previous studies. The results confirm previously postulated aspects of the BOLD mechanism in HSE experiments, and demonstrate the feasibility and advantages of HSE BOLD fMRI at 7 T for high-resolution functional mapping studies of the human brain.

MATERIALS AND METHODS

Investigation of HSE-Weighted BOLD Contrast

Eight normal subjects (five females and three males, 20–25 years old) participated in this study. All of the subjects provided informed consent to the experimental protocol, which was approved by the Institutional Review Board of the University of Minnesota. Each subject was studied once at 4 T and once at 7 T under similar experimental conditions, yielding a total of 16 studies.

The experiments were performed on a 7 T 90-cm bore system (Magnex Scientific, UK) for humans, or a 4 T 90-cm bore (Siemens, Germany), both of which were controlled by a Varian INOVA console (Varian Inc., Palo Alto, CA). The 7 T system was equipped with a head gradient insert (4 G/cm, 250 μs rise time) and the 4 T with the Sonata gradient set (4 G/cm, 400 μs rise time; Siemens). At both fields, a two-coil setup (9,24) consisting of a 6-cm quadrature surface coil for detection and a half-volume 14-cm quadrature surface coil for transmission was used for RF transmission and reception. This two-coil system allowed for sufficient B_1 homogeneity in the visual cortex for RF transmission, while preserving the SNR advantages of small reception coils.

TE and Field Dependence of BOLD Signal Changes (Without S-T Gradients)

To investigate the TE and field dependence of the signal changes (without diffusion weighting) during visual stimulation, HSE-weighted images were acquired from four subjects, once at 4 T and once at 7 T. This was done using a slice-selective 90° excitation pulse followed by a slab-selective (along the phase-encode) 180° refocusing pulse and an EPI readout (25,26). Four-millisecond sinc pulses were used for both the 90° and 180° pulses, with 2-ms crusher gradients of 2 G/cm placed around the refocusing pulse. Three chemical shift-selected (CHESS) pulses were used to suppress the fat signal. To achieve the desired TEs, partial Fourier acquisitions were used along the phase-encode direction. For a matrix size of 32 along the phase-encoding direction, 20 lines were acquired corresponding to k-space positions −4, −3, . . ., 14, and 15. The matrix size was 32 × 256, corresponding to a 1-mm resolution for an FOV of 3.2 cm × 25.6 cm. A 2-mm slice was selected along the calcarine fissure, and the slab width was ~3 cm for the FOV reduction along the phase-encoding direction. It should be noted that the techniques used in this study are currently only possible for a limited coverage of the human visual cortex. The TEs used were (in ms): 22, 42, 62, and 92 for 7 T, and 30, 50, 70, and 100 for 4 T. The TR was 2 s, and the EPI readout window was ~30 ms for both fields. While all functional series were acquired at an isotropic nominal in-plane resolution, the final resolution along the phase-encoding direction is expected to be somewhat degraded, because in EPI the readout windows typically have a duration comparable to the transverse relaxation constants. However, in all our functional series the total readout time was kept to ≤1.26 × T_2^* of the gray matter (either the true readout time in full Fourier imaging, or the equivalent total readout time in partial Fourier imaging). As a consequence, the FWHM approximation of the corresponding blurring filter along the phase-encoding direction in the EPI images was equal to or narrower than 0.54 pixels (27). A FWHM narrower than 1 pixel typically has a very limited impact on the final image resolution. Shimming was performed using FAST(EST) MAP (**f**ast

---

[1]Because the signal decay of blood water on the transverse plane is dominated by exchange and diffusion processes, it depends on the TE nonlinearly (i.e., the T_2 measured is itself TE-dependent) in an HSE sequence. Hence, we qualify the T_2 of blood as "apparent."

[2]In Ref. 16, calculations were made based on the susceptibility difference (hence the magnetic field difference) across the vessel boundary, for different levels of a contrast agent; however, this is equivalent to altering the magnetic field for a given susceptibility difference.

[3]These gradients are also known as "diffusion" gradients because they suppress signals from diffusing spins. However, in the body they also suppress blood signals due to the inhomogeneous blood velocities within a vessel and within a voxel.

automatic **s**him **t**echnique using **e**cho-planar **s**ignal read-**o**ut for **m**apping **a**long **p**rojections) (28), achieving water line widths of <20 Hz at 7 T and <15 Hz at 4 T over a 40 × 40 × 40 mm³ volume in the occipital lobe. For proper anatomic reference, a T_1-weighted image was acquired with inversion recovery-prepared EPI using acquisition parameters identical to those above except with a TR of 4 s. To minimize variation between subjects, the same subject was scanned at both fields and a similar slice was chosen in both sessions.

TE and Field Dependence of BOLD Signal Changes (With S-T Gradients)

In a separate study, the same protocol was used in the other four subjects (once at each field), with the addition of S-T gradients. The S-T gradients crush signals arising from large vessels due to inhomogeneous flow of blood in all vessels, and to the rapid diffusion of water in blood relative to that in tissue (29). In addition, when full relaxation is not achieved between consecutive acquisitions, S-T gradients also suppress the vascular component of "in-flow" effects coupled to activation. This enabled us to assess the field strength dependence of the extravascular BOLD signal changes around small vessels. In this study, a *b*-value of 100 s/mm² was used, and TEs of 37, 67, 87, and 107 ms were used for both fields. The S-T gradients were applied simultaneously along all three axes.

Investigation of Partial Volume Effects (PVEs) in HSE-Weighted BOLD fMRI

To investigate the nature of PVEs in our HSE-weighted (high-field) setup, three-segment (reduced FOV) images were acquired from two subjects with a 12.8 × 3.0 cm² FOV (256 × 60 matrix), yielding a 0.5-mm in-plane resolution. A 3-mm oblique axial slice along the calcarine fissure was imaged during visual stimulation. The TR/TE was 5 s/50 ms. The readout train per segment was also about ∼30 ms (20 phase-encode lines per segment, 1.5 ms per line).

Investigation of Inflow Effects in HSE-Weighted BOLD fMRI

To investigate the presence of any inflow effects from the 2-s repetition time (TR) used in these studies, two subjects were scanned with an MR acquisition protocol similar to that described above, using a TE of 67 ms at 7 T, with and without a nonselective adiabatic 90° pulse immediately following the data acquisition. This nonselective pulse eliminates effects caused by increases in blood flow induced by neuronal activity, because all spins, blood, and tissue are nulled for the entire sensitive volume of the large transmit coil.

Visual Stimulation Protocol

Visual stimulation was presented via a mirror placed over the subject's eyes, which allowed the subject to see a flashing (8 Hz) checkerboard matrix displayed on a screen behind the subject. The subject was presented with a flick-ering checkerboard pattern and asked to fixate on a point in the center of the matrix. Each epoch of the stimulus presentation consisted of a 20-s ON period and a 30-s OFF period. The epoch was repeated twice in a single run, and four to five runs (each lasting 2 min) were used for each TE. After each run, the subjects were allowed to relax their eyes for 1 min before beginning the next run. The same protocol was used in all of the above-mentioned studies, with the exception of the 0.5-mm resolution data. In that acquisition, the stimulus duration was 80 s, with an ON/OFF period of 40 s.

Data Processing and Analysis

The data were analyzed using routines written in PV-WAVE (Visual Numerics Inc., CO), and the STIMULATE software package (30) developed in our laboratory. Repeated runs of the same TEs were averaged before further data processing was performed. The data were zero-padded to a 256 × 256 matrix prior to being Fourier-transformed. Activation maps were generated using cross-correlation analysis of the response with the convolution of a boxcar with a hemodynamic response function (31). Assuming monoexponential dependence on TE, a log-linear least-squares regression was performed on a pixel by pixel basis to measure the apparent T_2 of tissue. To assess the TE dependence of the signal changes, the percent change from each subject at each TE was averaged separately for the data with and without S-T gradients, respectively. Gray matter ROIs were chosen based on the activated pixels detected at the TE = 92 or 107 ms data at 7 T, and matched to the corresponding locations in the 4 T scan using the anatomic images. The ROIs were closely matched using features of the T_1-weighted images. The long-TE map was used as a guide for the ROI selection to minimize selecting pixels originating largely from intravascular contributions. The same ROIs were used to analyze the TE dependence so that the same pixels were examined at all TEs, and similar anatomical locations were compared across the fields. For the field strength dependence, the ratios of percent changes observed at 7 T vs. those observed at 4 T were computed in the same subject, and then averaged across subjects on a TE basis. Percent changes at the two fields at similar TEs were compared with and without S-T gradients. For comparison purposes, the average percent change vs. TE of the data without S-T gradients were linearly interpolated to arrive at values for TEs used in the diffusion-weighted experiment. Our experimental data were compared with results from recent numerical work (32) simulating extravascular BOLD signal changes.

To assess any PVEs, the *k*-space of the high-resolution (0.5-mm) data were reconstructed using discrete Fourier transforms to yield different in-plane resolutions. In addition to reconstructing a 60 × 256 image (0.5 mm resolution), the data were reconstructed with the central 30 × 128, 16 × 64, and 8 × 16 *k*-space points to yield in-plane resolutions of 1.00 × 1.00 mm², 1.88 × 2.00 mm², and 3.75 × 4.00 mm², respectively. Zero-padding was used to ensure that the resultant images all had the same matrix size of 60 × 256. Activation maps were generated at each reconstructed resolution, and
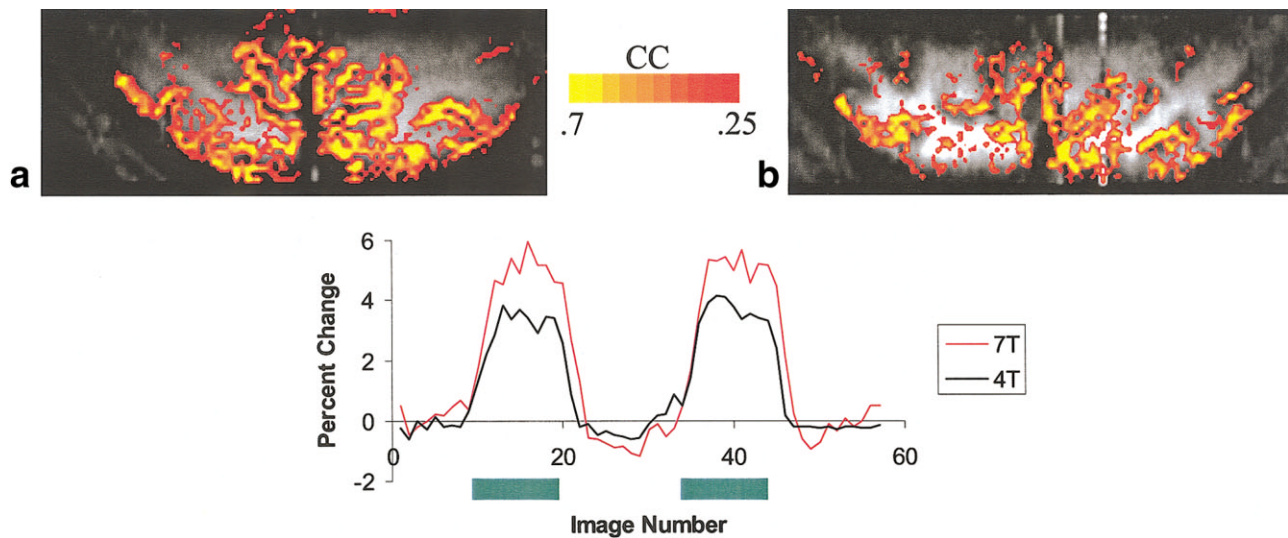
FIG. 1. Activation maps and their corresponding time courses from data from a single subject imaged at (**a**) 7 T at TE = 62 ms, and (**b**) 4 T at TE = 70 ms, overlaid on T_1-weighted anatomical images. The time courses, normalized to percent change, are shown below the respective maps. Maps from both fields were thresholded at the same significance ($P < .05$). The spatial resolution for both fields was 1 × 1 × 2 mm^3. The images displayed were zero-filled.

common activated pixels were compared across the different resolutions.

To evaluate the hypothesis that any observed changes in functional contrast with lower resolution are primarily due to a PVE between white and gray matter areas, we simulated the expected PVE. A gray matter ROI was selected based on the common activated pixels from the analysis of the real data. We first assumed that our selected ROI was gray matter, and that outside this ROI was not gray matter. The voxels contained in this ROI were set to one, while the remaining voxels were set to zero. This image was recreated 40 times and these images were denoted as OFF images. In a similar fashion, these same pixels within the ROI were set to 1.06, and zero outside; this image was recreated 20 times and the resulting images were denoted as ON images. A noise floor was then added to each individual image. The images were arranged as 20OFF-20ON-20OFF. The 60 images were reverse-Fourier-transformed to generate spatial frequency information and,

thereafter, reconstructed using Fourier transforms of portions of the k-space as in the experimental data analysis. The first reconstruction used the full k-space (60 × 256), while the subsequent reconstructions used only the center 30 × 128, 16 × 64, and 8 × 32 points of k-space, respectively. For these latter three cases, the k-space data was zero-filled to 60 × 256. The signal and signal changes over the predefined ROI were then calculated in the same fashion as with the experimental data. In addition, to mimic a more realistic situation, the same analysis was done with the pixels in the ROI set to 1.06 times a weighting function based on BOLD percent signal changes from the high-resolution data, and zero outside; this image was recreated 20 times and the resulting images were denoted as the ON images. Unlike the previous simulation, where activation in space was a step function, in this case it was a more realistic smooth function.

Finally, to quantify the relative contributions of inflow effects in our data at the TR used, average percent changes from an ROI were compared in the data acquired with vs.
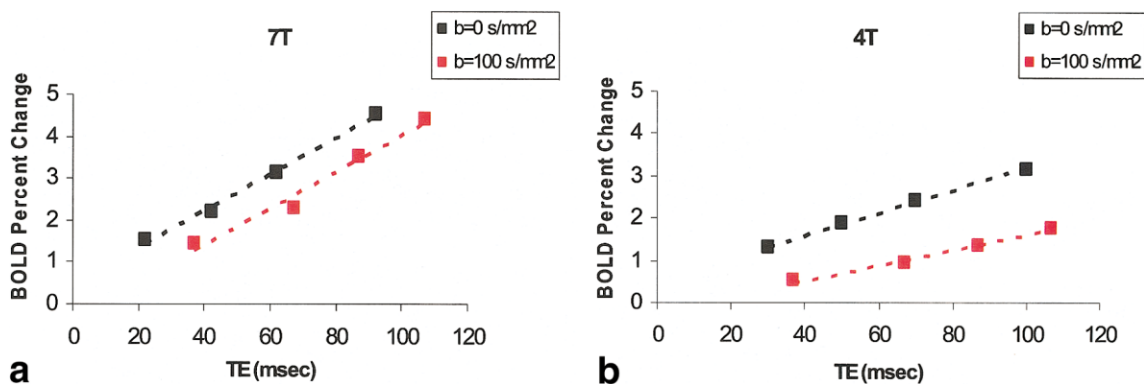

FIG. 2. Percent change vs. TE for (**a**) the 7 T data with and without S-T gradients, and (**b**) the 4 T data with and without S-T gradients. Plots represent the average of all the subjects' data from gray matter ROIs. The dotted line indicates a linear regression of the data.

Table 1
Summary of Calculated T_2 Values at 4 T and 7 T

	4 T	7 T
Gray matter T_2 (ms)	67.1 ± 6.0	55.0 ± 4.1
White matter T_2 (ms)	57.9 ± 3.8	45.9 ± 1.9

without the nonselective adiabatic 90° pulse following the readout.

RESULTS

Statistically significant activation was obtained at all TEs at both 4 and 7 T in all subjects. Percent changes of activated voxels ranged from 3% to 7%. An example of one subject's data at both 4 T and 7 T is presented in Fig. 1, in which the "activation" maps are overlaid on T_1-weighted HSE EPI images, and the average time course for those pixels considered as activated are plotted. The activation maps were thresholded at the same statistical confidence ($P < 0.05$) for both the 4 T and 7 T data (33). The 4 T activation map was generated from the 70-ms TE data, and the 7 T map was generated from the 62-ms TE data.

The results of the log-linear fitting of image signal intensity vs. TE to calculate T_2's of white matter and gray matter are summarized in Table 1. These numbers are in agreement with previous T_2 measurements (34). The small differences between the two studies may be the result of different acquisition parameters (i.e., spatial resolution) and/or imaging sequences. The TE dependence of percent signal change ($\Delta S/S$) detected by HSE BOLD with and without S-T gradients is plotted in Fig. 2 for the two field strengths. The TE dependence of $\Delta S/S$ was consistent with an approximately linear dependence, although some pixels did show a nonlinear dependence. In addition, as evidenced in Fig. 2, the slope of the TE dependence is significantly different with and without diffusion gradients in the 4 T data, and not in the 7 T data. Unlike the 4 T data, the slope of the TE dependence was not affected by the applications of the S-T gradients to suppress the blood contribution. However, there was an effect on the intercept, indicating that there is an "inflow" component that is eliminated by the S-T gradients.

Results from the field strength dependence analysis are summarized in Fig. 3. The fractional change induced by visual stimulation ($\Delta S/S$) at 7 T relative to 4 T obtained without S-T gradients was similar at all TEs. However, it increased slightly with TE, which suggests that the 4 T contrast is relatively more attenuated by TE, probably as a result of slower suppression of the blood contribution with increasing TE. The ratio of 7 T vs. 4 T percent changes without S-T gradients was 1.51 ± 0.25. However, when S-T gradients were employed to reduce the contribution of blood, this ratio increased to 2.6 ± 0.26, which is close to the predicted value of 3 for a quadratic dependence on magnetic field (17), and is in full agreement with the
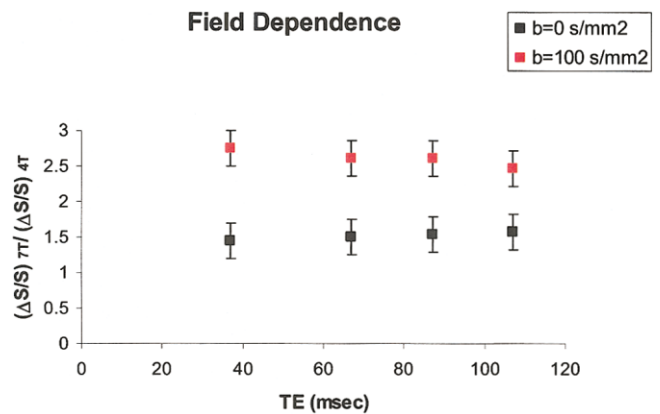

FIG. 3. Plot of the ratio $(\Delta S/S)_{7T}/(\Delta S/S)_{4T}$ of the average percent changes vs. TE with and without S-T gradients. Plots represent the average of all the subjects' data from gray matter ROIs.

2.8 dependence predicted by Fujita (32) for a 3-μm-radius blood vessel.[4]

Figure 4 shows how our data fits with a numerical model from a recent study (32) of extravascular BOLD signal changes vs. TE for a 3-μm-radius vessel. The data are fit using vascular volume as the adjustable parameter. As shown in Fig. 4, the data with S-T gradients agreed well with the simulation for both the 4 T and 7 T data. The data led to a vascular volume fraction of 1.5% at 7T and 2.2% at 4T, consistent with blood volume occupied by capillaries in gray matter (35).

The data obtained with high resolution were reconstructed at lower in-plane resolutions. A monotonic decrease in the percent change was seen with decreasing spatial resolution (see Fig. 5). When the voxel size approached the typical fMRI resolutions ($3 \times 3 \times 5$ mm^3 = 45 mm^3), the percent changes were reduced by nearly a factor of 2. In the PVE, for both the smooth distribution and the step function of activation, the signal loss of the predefined gray matter areas results in a corresponding

---

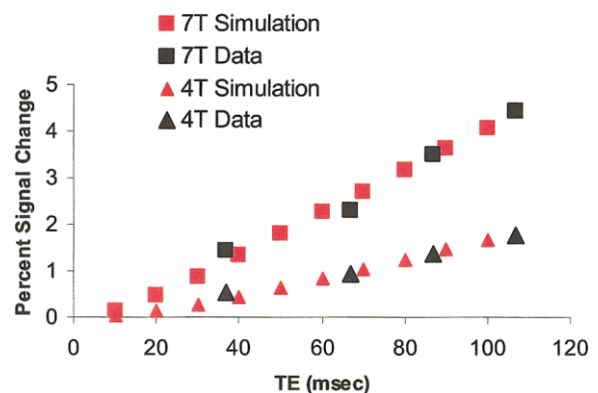[4]The average capillary diameter in the cat visual cortex was reported to be 5.1 ± 0.86 μm (35).

FIG. 4. Plot of simulated extravascular BOLD signal changes vs. TE, and the fit of our S-T weighted data for the respective fields (CBV = 2.2% (4 T), 1.5% (7 T)).
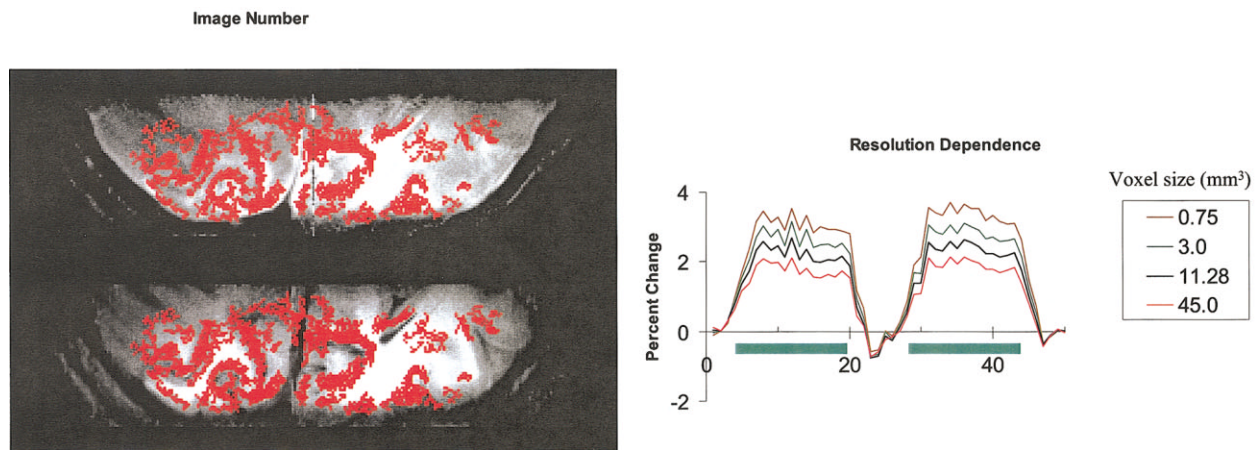
FIG. 5. Time course of activated pixels reconstructed at different in-plane resolutions from the original data (7 T) acquired with 0.5×0.5 mm^2 nominal in-plane resolution and 3-mm slice thickness. Brown (original data) = 0.75 mm^3, green = 3 mm^3, black = 11.28 mm^3, and red = 45 mm^3. The activation map is shown overlaid on both the reconstructed T_2-weighted EPI image (0.75 mm^3 voxels) and the T_1-weighted EPI image. The map represents common activated pixels from each of the reconstructed resolutions.

loss in contrast as a function of in-plane resolution. The comparison of the smooth distribution and the experimental data is depicted in Fig. 6. The functional form of the simulated loss in contrast (due to PVE) vs. resolution closely follows that of the experimental results.

Finally, the data acquired with and without a nonselective adiabatic 90° pulse immediately following the image acquisition to eliminate the inflow problem did not show a large difference in the amount of HSE BOLD activation. The activation in the flow-suppressed data obtained using the adiabatic 90° postacquisition pulse was 87.7% ± 3.8% that of the non-flow-suppressed data at 7T. This was in agreement with the intercept of the plot shown in Fig. 2 without S-T gradients, and supports the notion that the intercept was reduced to approximately zero by the flow-suppressing S-T gradients.

DISCUSSION

Magnetic Field Dependence of the HSE BOLD Effect Magnitude

As discussed in the Introduction, the HSE BOLD effect arises from extravascular tissue spins around the micro-
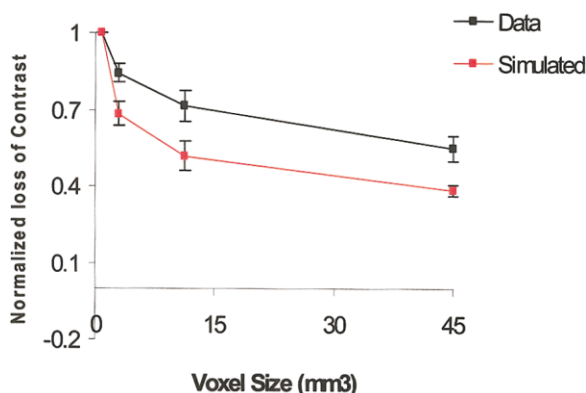

FIG. 6. The experimental results of contrast loss as a function of resolution, overlaid with the simulated results. The activation is normalized to one at the highest resolution.

vasculature and from intravascular blood spins. The blood contribution is suppressed at high magnetic fields because the apparent T_2 of blood shortens dramatically with increasing fields, from 180 ms at 1.5 T (36) to 20 ms at 4 T and ~7 ms at 7 T (9) (depending on the O_2 saturation), while the gray matter T_2 decreases slightly, from ~80 to 90 ms at 1.5 T (37) to 67 ms and 55 ms at 4 T and 7 T, respectively. Therefore, at TEs comparable to the T_2 of tissue, the blood signal is greatly diminished at high fields and is expected to contribute negligibly to the HSE BOLD contrast.

Without the confounding contributions from the intravascular BOLD and "inflow" effects, HSE BOLD contrast associated with the extravascular spins is expected to increase supralinearly with magnetic field magnitude. The ratio between 4 T and 7 T, the two fields used in this study, was approximately linear in the absence of S-T gradients to suppress the blood signals. This ratio became supralinear and was equal to 2.6 in the presence of S-T gradients. This is consistent with the expectation that the contribution of BOLD signals originating from blood is significantly larger at 4 T than at 7 T. The notion of a larger intravascular signal at 4 T was also supported by observations that the ratio between the fields tended to increase with longer TEs, which would result in diminished blood signals, and the S-T gradients altered the slope of the TE dependence significantly at 4 T and not at 7 T.

Modeling studies (17) have predicted a quadratic dependence on the magnetic field magnitude for a population of vessels with radii less than ~5–8 μm when the susceptibility-induced frequency difference between cylinders representing the blood vessels and their surrounding space was 64 or 32 Hz, respectively. For the field strengths studied here, a quadratic dependence would yield a ratio of 3. A slightly less than quadratic dependence (2.8-fold vs. threefold) is expected, according to Fujita (32), for a 3-μm-radius vessel. Our experimentally determined value of 2.6 between 4 T and 7 T approaches that predicted by Fujita. There are, however, several reasons why the experimental measurements of the type performed in this study will *underestimate* this ratio compared to modeling re-

sults. First, while S-T gradients suppress signals from the blood, they do not necessarily eliminate them completely. Thus, a blood contribution to the BOLD effect may persist at 4 T even in the presence of these gradients, while it is suppressed at the 7 T field because of the short venous blood T_2. In addition, the size distribution of the blood vessels that contribute to the extravascular BOLD effect in HSE fMRI will not remain the same at the two fields. Simulations suggest that as the magnetic field difference between the vessel interior and the extravascular space increases, the dynamic averaging regime shifts to smaller vessels (16,17). Thus, while the contribution is smaller from the *same*-size vessels at 4 T compared to 7 T, slightly larger vessels, such as venules, are expected to contribute more to the T_2 change at 4 T relative to 7 T. Consistent with this explanation, the vascular volume contribution calculated by fitting the data to a model was greater at 4 T than at 7 T.

The TE dependence was shown to be approximately linear. When compared to the results of Fujita (32), our data agreed remarkably well with the 3-μm-radius vessel simulation, corresponding to a vascular volume of 1.5% for 7 T and 2.2% for 4 T for the blood-suppressed data obtained with the S-T gradients. These are in excellent agreement with the capillary volume of ~2% in cortical gray matter (35), and support the claim that HSE BOLD signals arise predominantly from the capillaries.

The capillary (hence gray matter) origin of the signals is also supported by the dependence of signal intensity changes on voxel dimensions (Figs. 5 and 6). If the source of the activation signals is the gray matter, the PVE with surrounding white matter and CSF space will affect the percent signal intensity change observed. Given the fact that the gray matter in the human brain is a highly curved ribbon (1–2 mm thick), the elimination of PVE would require relatively high resolution. In the current study, the percent signal changes in HSE fMRI following visual stimulation were between 3% and 7% in statistically significant voxels, and monotonically increased with higher spatial resolution, indicating that there are PVEs. Our simulations (see Fig. 6) supported the conclusion that this PVE stemmed from the dilution of gray matter within a voxel by surrounding tissue and CSF space. A recent study (11) also found similar significant increases in contrast when using high spatial resolutions in perfusion-based functional imaging. This is consistent with the HSE data reported here. With appropriately long tagging times, perfusion functional images suppress large vessel effects and arise from water flow into capillaries, and, by exchange across capillary walls, into tissue. In the absence of macrovascular contribution, perfusion functional images must also be restricted to the gray matter, since the basal blood flow and blood flow increases with activation are higher in gray matter.

A recent experimental study of GRE BOLD fMRI at 3 T (38) revealed that the total activated volume passing a given threshold (and percent signal change) peaked at an isotropic resolution of 1.5 mm and subsequently decreased. This was attributed to the spatial distribution of small veins in the cortical gray matter and PVEs with larger voxel sizes. For 7 T HSE BOLD, where the source of the signals is even smaller vessels (i.e., capillaries), the

percent changes should continue to increase for voxels < 1.5 mm. This is indeed what was observed here (Figs. 5 and 6). Capillary level activation is expected to become independent of voxel size when the voxels are small enough that they can be fully occupied by gray matter without PVEs from neighboring white matter and CSF space. Only after this condition is achieved will they be independent of voxel volume, until the voxel dimensions are reduced to dimensions comparable to the intercapillary distance of ~25 μ (35). Therefore, a maximum signal change is not expected at approximately 1.5 mm isotropic resolution, and was not seen at 7 T using HSE BOLD.

Non-T_2-Related Effects on HSE BOLD Images

The HSE functional images presented here can contain contributions from effects other than the HSE BOLD mechanism. Full relaxation is not attained between consecutive excitation pulses, resulting in inflow effects, and finite readout times in the EPI acquisition results in T_2' effects (i.e., $(1/T_2^*) = (1/T_2) + (1/T_2')$). The intercept of the linear extrapolation of the HSE BOLD percent change vs. TE without S-T gradients is a direct experimental measure of the sum of all possible non-T_2 effects. In the studies reported here, this corresponded to a ~0.3–0.4% signal change, or ~10–15% of the total HSE BOLD activation. The data acquired with and without the nonselective adiabatic 90° pulse after the readout suggested independently that, in the current data, ~12% of the BOLD changes at 7 T may be related to inflowing spins. A somewhat smaller contribution is expected at 4 T, where the T_1 is shorter. This suggests that most of the non-T_2 contribution yielding the nonzero intercept in percent change vs. TE is due to inflow and not the finite readout window of the EPI sequence. Consistent with this conclusion, S-T gradients virtually eliminated this nonzero intercept. This small inflow component can, in principle, have both tissue (i.e., perfusion) and macrovascular flow components; however, given the relatively long TR used, they are expected to be associated primarily with microvasculature.

As previously mentioned, the total readout durations (or the equivalent total readout durations in partial Fourier) were about 1.2 times the T_2^*'s of gray matter at both fields. Thus, the amount of T_2' contamination was partially balanced between both fields in this case. The complete, multiparameter description of the T_2' contribution in spin-echo EPI is actually quite complex and is beyond the scope of this work. It should be noted that in our data the size of the activation is large compared to the image. Therefore, the central *k*-space points contain most of the information (relative to other studies, in which the activation volume was small compared to the FOV), and T_2' effects are more prominent.

Specificity of HSE vs. GRE BOLD Images at 7 T

The blood effects that cause spatially inaccurate activation are most prominent when the blood volume occupies a significant fraction of the voxel volume; thus, the source of false activation can extend from the draining blood vessels (one to several millimeters in diameter) that can be distant from the site of activation (7,8,12) by as much as centime-

ters. This occurs even though these macroscopic veins (some of which remain at their basal level of activity during the stimulation or task period) pool blood from a large cortical territory, thereby diluting the alteration in the deoxyhemoglobin concentration caused by the activated sites. A clear example of such false activation associated with large vessels is the apparent but false activation seen in the sagittal sinus, which is one of the largest draining veins in the brain, and which pools blood from the frontal lobes to the visual cortex (see, for example, 4.7 T visual stimulation data in the cat cortex) (8,12). These distant large vessel effects are largely suppressed at 7 T (9,11) or 9.4 T (22) compared to lower fields because of the dramatically shorter T_2 of blood, *provided* the TEs used are long compared to the apparent blood T_2. However, even when the blood effects are mostly eliminated, extravascular effects can persist, especially in the small venules and veins that immediately follow the capillaries. This effect is proportional to the product of the blood volume and the susceptibility gradient across the blood vessel (17). Therefore, whether or not extravascular effects from larger vessels remain in GRE BOLD images depends on 1) the blood volume in a particular voxel, 2) the magnitude of the susceptibility change caused by the activation at the active site, and 3) the extent of pooling of blood from the activated site with blood from regions that remain in their basal state of activity as blood flows away from the active site. Thus, it is possible for maximal visual stimulation to result in extravascular effects from large vessels in GRE fMRI at 7 T; however, the same large vessels may not be detectable if the contrast of the stimulus is reduced significantly.

The presence of residual contributions from larger-than-capillary venous vessels in GRE fMRI even at 7 T can be surmised from the fact that the field dependence of the ΔR_2^* for gray matter regions increased only ~2.1-fold going from 4 T to 7 T (9) even when the large vessel areas visible at the image resolution were excluded. This is significantly less than what we observed in this HSE study. We have also previously shown in rat brain images at 9.4 T that while perfusion-based fMRI maps agreed well with sites of Mn^{++} uptake associated with synaptic activity, and colocalized to middle layers of the gray matter with maximum effect at layer 4, the GRE BOLD images displayed maximum signal on or near the cortical surface, where the larger draining vessels are located (15). Similarly, a recent high-resolution study in humans, conducted at 7 T (11), showed that perfusion-based functional maps, obtained with sufficiently long tagging delays to ensure predominantly microvascular and tissue contribution, were confined to the gray matter ribbon; however, the GRE BOLD images had the largest increases in the sulci immediately adjacent to activated gray matter regions, presumably again due to the extravascular dephasing induced by postcapillary draining vessels on the cortical surface.

Within the cortical gray matter are 50–100-μ veins, separated by 1–1.5 mm, that drain the capillaries. These are the blood vessels that can be seen in high-resolution T_2^*-weighted images as dark lines traversing the gray matter perpendicular to the cortical surface (39). These small veins drain immediately into similarly-sized or somewhat larger veins on the cortical surface. Because these vessels

drain a small territory, the deoxyhemoglobin alterations induced at the active site at the terminal ends of the capillaries are mostly, if not fully, preserved in going from capillaries to these small-diameter postcapillary vessels. Consequently, these small intracortical and surface venules and veins must have a significant extravascular effect—one that must exceed the capillary contribution to extravascular BOLD, since, unlike the capillaries, they are large enough to be outside the dynamic averaging regime that diminishes the BOLD effect (and, hence, converts it from a T_2^* to an apparent T_2 phenomenon). The small veins located on the cortical surface are likely the source of intense but false activation seen within sulci in human GRE BOLD images at 7 T (11). Their contribution to the GRE BOLD images at 7 T would be suppressed in HSE images, which originate, according to our data, from the capillaries. In addition, however, the intracortical draining veins will also be suppressed in HSE fMRI. This suppression would be critical for mapping functional parcellation on the submillimeter scale and across different layers in the gray matter. Consistent with this, the activation follows the cortical gray matter in the HSE images (Fig. 1), with the largest intensity in the middle layers rather than in the outer surface and in the intrasulcal space. The appearance of the greatest intensity in the middle layers (rather than the cortical surface) is expected, since the inputs from the lateral geniculate nuclei terminate in layer 4.

In addition to the differential extravascular BOLD contribution expected for HSE and GRE fMRI at 7T, the intravascular contribution cannot necessarily be assumed to be equally suppressed by the two approaches at the same field strength. This is because the TEs used in the two approaches are not the same. In the HSE acquisition, TE values of ~50 to ~60 ms can easily be employed since tissue T_2 is ~55 ms. However, tissue T_2^* is ~25 ms in the visual cortex, restricting the maximal TE values that can be practically used to ~25 ms. In places near the air-filled cavities, this cannot be attained. Even with a 25-ms TE, however, a small, residual blood contribution can remain in GRE experiments, as shown in our previous work (9). If shorter TEs are used for improved image SNR, especially in regions where magnetic field homogeneity is poor (such as near air-filled cavities), the large vessel effects will "propagate" further down the venous tree toward major draining veins, because of larger intravascular contributions at the shorter TEs.

Whether the specificity gains discussed above for HSE images vs. GRE images at 7 T are important will depend on the spatial scale of the functional questions under investigation. Clearly, millimeter- to submillimeter-scale functional organizations may be outside the reach of GRE BOLD unless differential imaging strategies to eliminate nonspecific activation can be employed. However, the spatial scale of the nonspecificity in the GRE BOLD images at 7 T remains to be determined, and is beyond the scope of this work.

Specificity of 7 T HSE BOLD Images Compared to Lower-Field HSE and GRE BOLD Images

When the apparent T_2 of blood is significantly shorter than gray matter T_2, the spatially nonspecific blood effect in

HSE fMRI images can be suppressed by going to TEs that are long relative to apparent blood T_2 but are short enough to retain significant gray matter signals in the image. This can clearly be accomplished at 7 T, and even at 4 T, albeit with less efficiency. However, at 3 T and below, this mechanism becomes increasingly inoperative. At 1.5 T, the most widely available and frequently used field strength in fMRI studies, the apparent blood T_2 is in fact approximately two- to threefold longer (36) than the tissue T_2. Therefore, it would be impossible to suppress the blood contribution by going to long TEs. In GRE BOLD images, where shorter TEs must be employed due to the shorter $T_2^\star$ relative to T_2, the blood contribution will be present even at 4 T (9). Thus, 7 T HSE fMRI is expected to have significantly better specificity compared to that achieved at lower fields. Only at field strengths of ∼4 T and above can one obtain a specificity in HSE (but not GRE) images similar to that observed at 7 T by using sufficiently long TEs to reduce the blood contribution. In this case, the advantage of imaging at 7 T is not so much the specificity achieved, but rather the significantly increased CNR due to the virtually quadratic increase in the capillary BOLD effect with magnetic field, and the gains in intrinsic SNR of images.

These conclusions are supported by data obtained at the lower fields. Oja et al. (1, p. 617) found that "when using the standard resolution for fMRI studies at 1.5 T, the effects of spin-echo changes in the draining veins are of major contribution to the total [HSE] BOLD signal changes measured in voxels encompassing the activated brain areas." These intravascular blood effects dominate even the GRE fMRI images at 1.5 T, as demonstrated in experiments using S-T gradients (2,4). Similarly, based on HSE and GRE studies that incorporated inversion recovery prior to signal excitation, the role of spin dephasing around capillaries in gray matter was found to be insignificant at 1.5 T fMRI (3). Instead, the fMRI signal changes were ascribed to extravascular dephasing effects in both gray matter and CSF around a venous vessel (that would be detected in GRE BOLD images), in combination with intravascular effects that would contribute to both GRE and HSE fMRI (3). At 3 T, perfusion-based fMRI maps, which are expected to yield microvascular and gray matter activation, did not overlap more than 40% with HSE functional images (40), which indicates that macrovascular contributions that would arise from intravascular blood-related effects remain as a large effect at this field strength. Consistent with this, the intravascular blood contribution was found to be 50% in HSE BOLD images at 3 T (20). In addition, it was concluded that in the human visual cortex, BOLD signal changes at 3 T have contributions from the extravascular space and larger blood vessels in roughly equal amounts.

CONCLUSIONS

Robust BOLD responses, acquired with Hahn spin echoes and EPI readouts, were detected at high spatial resolutions at 4 T and 7 T. In good agreement with theoretical predictions (17,32), the experimental results indicate that there is a supralinear increase in the HSE BOLD contrast when going from 4 T to 7 T if the confounding and undesirable effects of the intravascular (blood) BOLD effect are suppressed. Apparent T_2 values of tissue for an HSE sequence were measured at both fields. Together with earlier data (9), these measurements show that the relative difference between apparent HSE T_2 values of tissue and blood is significantly greater at high fields. This phenomenon results in a reduced blood contribution at TEs that are equal to the tissue HSE T_2 for fMRI at higher fields, which is the optimum TE when "noise" in fMRI data is not proportional to signal, as expected for high-resolution studies in which MR noise dominates. Finally, the linear dependence of the signal changes with TE is in good agreement with a recent theoretical model (32), and with the capillary origin of the signals. These results indicate that HSE BOLD contrast at high magnetic fields represents a viable method for high-resolution and high-specificity functional mapping.

REFERENCES

1. Oja JME, Gillen J, Kauppinen RA, Kraut M, van Zijl PCM. Venous blood effects in spin-echo fMRI of human brain. Magn Reson Med 1999;42:617–626.
2. Song AW, Wong EC, Tan SG, Hyde JS. Diffusion weighted fMRI at 1.5 T. Magn Reson Med 1996;35:155–158.
3. Hoogenraad FG, Pouwels PJ, Hofman MB, Reichenbach JR, Sprenger M, Haacke EM. Quantitative differentiation between BOLD models in fMRI. Magn Reson Med 2001;45:233–246.
4. Boxerman JL, Bandettini PA, Kwong KK, Baker JR, Davis TJ, Rosen BR, Weisskoff RM. The intravascular contribution to fMRI signal changes: Monte Carlo modeling and diffusion-weighted studies in vivo. Magn Reson Med 1995;34:4–10.
5. Frahm J, Merboldt KD, Hanicke W, Kleinschmidt A, Boecker H. Brain or vein-oxygenation or flow? On signal physiology in functional MRI of human brain activation. NMR Biomed 1994;7:45–53.
6. Duyn JH, Moonen CTW, Yperen GH, Boer RW, Luyten PR. Inflow vs. deoxyhemoglobin effects in BOLD functional MRI using gradient echoes at 1.5T. NMR Biomed 1994;7:83–88.
7. Menon RS, Ogawa S, Tank DW, Ugurbil K. 4 Tesla gradient recalled echo characteristics of photic stimulation-induced signal changes in the human primary visual cortex. Magn Reson Med 1993;30:380–386.
8. Duong TQ, Kim DS, Ugurbil K, Kim SG. Spatio-temporal dynamics of the BOLD fMRI signals: toward mapping submillimeter cortical columns using the early negative response. Magn Reson Med 2000;44:231–242.
9. Yacoub E, Shmuel A, Pfeuffer J, Van de Moortele P-F, Adriany G, Andersen P, Vaughan J, Merkle H, Ugurbil K, Hu X. Imaging brain function in humans at 7 Tesla. Magn Reson Med 2001;45:588–594.
10. Ugurbil K, Hu X, Chen W, Zhu XH, Kim SG, Georgopoulos A. Functional mapping in the human brain using high magnetic fields. Philos Trans R Soc Lond Biol Sci 1999;354:1195–1213.
11. Pfeuffer J, Adriany G, Shmuel A, Yacoub E, Van De Moortele PF, Hu X, Ugurbil K. Perfusion-based high-resolution functional imaging in the human brain at 7 Tesla. Magn Reson Med 2002;47:903–911.
12. Kim D-S, Duong T, Kim S-G. High-resolution mapping of iso-orientation columns by fMRI. Nat Neurosci 2000;3:164–169.
13. Malonek D, Grinvald A. Interactions between electrical activity and cortical microcirculation revealed by imaging spectroscopy: implications for functional brain mapping. Science 1996;272:551–554.
14. Yacoub E, Shmuel A, Pfeuffer J, Van de Moortele PF, Adriany G, Ugurbil K, Hu X. Investigation of the initial dip in fMRI at 7 Tesla. NMR Biomed 2001;14:408–412.
15. Duong TQ, Kim DS, Ugurbil K, Kim SG. Localized cerebral blood flow response at submillimeter columnar resolution. Proc Natl Acad Sci USA 2001;98:10904–10909.

16. Boxerman JL, Hamberg LM, Rosen BR, Weisskoff RM. MR contrast due to intravscular magnetic susceptiblity perturbations. Magn Reson Med 1995;34:555–556.

17. Ogawa S, Menon RS, Tank DW, Kim S-G, Merkle H, Ellermann JM, Ugurbil K. Functional brain mapping by blood oxygenation level-dependent contrast magnetic resonance imaging. Biophys J 1993;64:800–812.

18. Gao J, Xiong J, Schiff LJ, Roby J, Lancaster J, Fox P. Fast spin-echo characteristics of visual stimulation-induced signal changes in the human brain. J Magn Reson Imaging 1995;5:709–714.

19. Constable R, Kennan R, Puce A, McCarthy G, Gore J. Functional NMR imaging using fast spin echo at 1.5 T. Magn Reson Med 1994;31:686–690.

20. Norris DG, Zysset S, Mildner T, Wiggins CJ. An investigation of the value of spin-echo-based fMRI using a Stroop color-word matching task and EPI at 3 T. Neuroimage 2002;15:719–726.

21. Thulborn KR, Waterton JC, Mattews PM, Radda GK. Oxygenation dependence of the transverse relaxation time of water protons in whole blood at high field. Biochem Biophys Acta 1982;714:265–270.

22. Lee S-P, Silva A, Ugurbil K, Kim S-G. Diffusion-weighted spin-echo fMRI at 9.4T: microvascular/tissue contribution to BOLD signal changes. Magn Reson Med 1999;42:919–928.

23. Stejskal E, Tanner J. Spin diffusion measurements: spin echoes in the presence of a time-dependent field gradient. J Chem Phys 1965;42:288–292.

24. Adriany G, Pfeuffer J, Yacoub E, Van de Moortele P-F, Shmuel A, Andersen P, Hu X, Vaughan JT, Ugurbil K. A half-volume transmit/receive coil combination for 7 Tesla applications. In: Proceedings of the 9th Annual Meeting of ISMRM, Glasgow, Scotland, 2001. p 1097.

25. Duong TQ, Yacoub E, Adriany G, Hu X, Ugurbil K, Kim S-G. High-resolution, spin-echo BOLD and CBF fMRI: single-shot, slab-selective EPI. Magn Reson Med 2002;48:589–593.

26. Yang Y, Mattay V, Weinberger D, Frank J. Localized echo-volume imaging—methods for functional MRI. J Magn Reson Imaging 1997;7:371–375.

27. Haacke EM, Brown RW, Thompson MR, Venkatesan R. Magnetic resonance imaging: physical principles and sequence design. New York: John Wiley & Sons, Inc.; 1999.

28. Gruetter R, Tkac I. Field mapping without reference scan using asymmetric echo-planar techniques. Magn Reson Med 2000;43:319–324.

29. Fisel CR, Ackerman JL, Buxton RB, Garrido L, Belliveau JW, Rosen BR, Brady TJ. MR contrast due to microscopically heterogeneous magnetic susceptibility: numerical simulations and applications to cerebral physiology. Magn Reson Med 1991;17:336–347.

30. Strupp JP. Stimulate: a GUI based fMRI analysis software package. NeuroImage 1996;3:S607.

31. Friston K, Jezzard P, Turner R. Analysis of functional MRI time series. Hum Brain Mapp 1994;1:153–171.

32. Fujita N. Extravascular contribution of blood oxygenation level dependent signal changes: a numerical analysis based on a vascular network model. Magn Reson Med 2001;46:723–734.

33. Bandettini PA, Jesmanowicz A, Wong EC, Hyde JS. Processing strategies for time-course data sets in functional MRI of the human brain. Magn Reson Med 1993;30:161–173.

34. Bartha R, Michaeli S, Merkle H, Adriany G, Andersen P, Chen W, Ugurbil K, Garwood M. In vivo 1H2O T_2+ measurement in the human occipital lobe at 4T and 7T by Carr-Purcell MRI: detection of microscopic susceptibility contrast. Magn Reson Med 2002;47:742–750.

35. Pawlik G, Rackl A, Bing RJ. Quantitative capillary topography and blood flow in the cerebral cortex of cats: an in vivo microscopic study. Brain Res 1981;208:35–58.

36. Barth M, Moser E. Proton NMR relaxation times of human blood samples at 1.5 T and implications for functional MRI. Cell Mol Biol 1997;43:783–791.

37. Breger RK, Rimm AA, Fischer ME, Papke RA, Haughten VM. T_1 and T_2 measurements on a 1.5 Tesla commercial imager. Radiology 1989;171:273–276.

38. Hyde JS, Biswal B, Jesmanowicz A. High-resolution fMRI using multi-slice partial k-space GR-EPI with cubic voxels. Magn Reson Med 2001;46:114–125.

39. Ogawa S, Lee T-M. Magnetic resonance imaging of blood vessels at high fields: in vivo and in vitro measurements and image simulation. Magn Reson Med 1990;16:9–18.

40. Luh WM, Wong EC, Bandettini PA, Ward BD, Hyde JS. Comparison of simultaneously measured perfusion and BOLD signal increases during brain activation with T(1)-based tissue identification. Magn Reson Med 2000;44:137–143.